

NJC

Accepted Manuscript



This is an *Accepted Manuscript*, which has been through the Royal Society of Chemistry peer review process and has been accepted for publication.

Accepted Manuscripts are published online shortly after acceptance, before technical editing, formatting and proof reading. Using this free service, authors can make their results available to the community, in citable form, before we publish the edited article. We will replace this *Accepted Manuscript* with the edited and formatted *Advance Article* as soon as it is available.

You can find more information about *Accepted Manuscripts* in the [Information for Authors](#).

Please note that technical editing may introduce minor changes to the text and/or graphics, which may alter content. The journal's standard [Terms & Conditions](#) and the [Ethical guidelines](#) still apply. In no event shall the Royal Society of Chemistry be held responsible for any errors or omissions in this *Accepted Manuscript* or any consequences arising from the use of any information it contains.

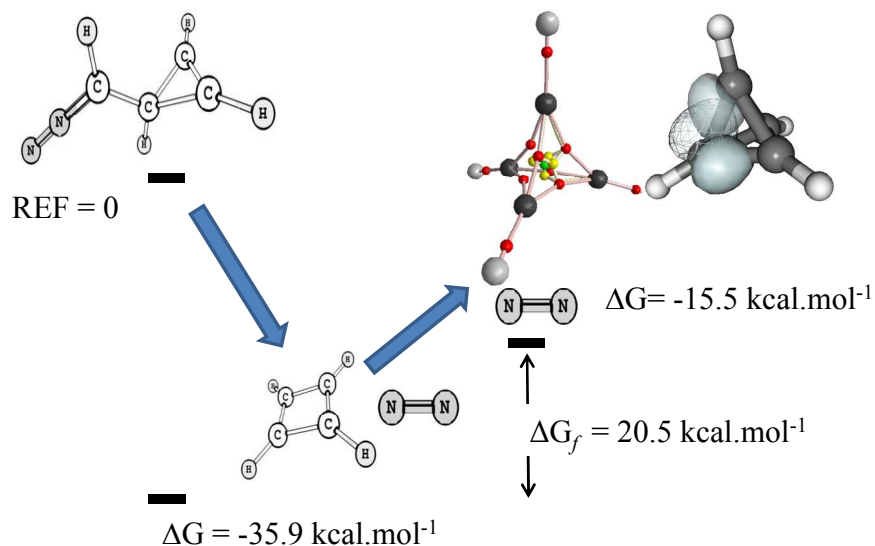
Stability and Electronic Structure of Substituted Tetrahedranes, Silicon and Germanium Parents – a DFT, ADMP, QTAIM and GVB study (REVISED)

Norberto K. V. Monteiro, José F. de Oliveira and Caio L. Firme*

Institute of Chemistry, Federal University of Rio Grande do Norte, Natal-RN, Brazil, CEP 59078-970.

*Corresponding author. Tel: +55-84-3215-3828; e-mail: caiofirme@quimica.ufrn.br

Graphical Abstract



Abstract

The electronic structure and the stability of tetrahedrane, substituted tetrahedranes and silicon and germanium parents have been studied at ω B97XD/6-311++G(d,p) level of theory. The quantum theory of atoms in molecules (QTAIM) was used to evaluate the substituent effect on the carbon cage in the tetrahedrane derivatives. The results indicate that electron withdrawing groups (EWG) have two different behaviors, i.e., stronger EWG makes the tetrahedrane cage slightly unstable while slight EWG causes a greater instability in the tetrahedrane cage. On the other hand, the sigma electron donating groups, σ -EDG, stabilizes the tetrahedrane cage and π -EDG leads to tetrahedrane disruption. NICS and D3BIA indices were used to evaluate the sigma aromaticity of the studied molecules, where EWGs and EDGs results in decrease and increase, respectively, of both aromaticity indices, showing that sigma aromaticity plays an important role in the stability of tetrahedrane derivatives. Moreover, for tetra-*tert*-butyltetrahedrane there is another stability factor: hydrogen-hydrogen bonds which imparts a high stabilization in this cage. Generalized valence bond (GVB) was also used to explain the stability effect of the substituents directly bonded to the carbon of the tetrahedrane cage. Moreover, the ADMP simulations are in accordance with our thermodynamic results indicating the unstable and stable cages under dynamic simulation.

Keywords: Tetrahedrane; QTAIM; NICS; D3BIA; GVB; ADMP

1. Introduction

The development of new high energy molecules has aroused great interest of theoreticians and experimentalists, with applications in the military industry and others high-tech fields.¹ Cage strained organic molecules can be used as potential explosives in response to various external stimuli such heat, shock or impact.¹⁻⁴ The highly-strained cage compounds have raised interest due to their high density and high energy. As a consequence, they can also be used as energetic materials, such as hexanitrohexaazaisowurtzitane^{1,5} and octanitrocubane.⁶ Similarly, tetrahedrane is also a high-energy molecule. Despite many attempts to isolate the parent tetrahedron (unsubstituted – C₄H₄) were not successful,⁷ Maier *et al*⁸ in 1978 were able to synthesize the first tetrahedrane derivative, the tetra-*tert*-butyltetrahedrane.

Tetrahedrane is one of the most strained organic molecule, with highly symmetrical structure and unusual bonding being known as a Platonic solid. It has a strain energy of 586 kJ.mol⁻¹ according to Wiberg *et al*⁹ which makes this compound thermodynamically unstable. As a consequence, their synthesis and isolation tends to be extremely difficult. Conversely, tetrahedrane has σ -aromaticity¹⁰ because it has a large negative NICS (Nucleus Independent Chemical Shift) value, which can somehow contribute for decreasing the high instability of tetrahedrane cage.

Tetrahedrane and its derivatives can be obtained from the corresponding cyclobutadiene or derivatives. The anti-aromatic and highly-reactive cyclobutadiene has only been isolated at low temperature in inert matrices¹¹ and immobilized more recently at room temperature in hemicarcerand.¹² On the other hand, structural parameters of substituted cyclobutadienes have been reported showing pronounced bond alternations,^{13,14} although only slight CC bond length alternations (1.464 and 1.482 Å), under room temperature, of tetrakis (*tert*-butyl) cyclobutadiene¹⁵ have been reported. In fact, measurements at -150 °C showed noticeably larger bond alternation (1.441 and 1.526 Å) for tetrakis (*tert*-butyl) cyclobutadiene as well.

Tetra-*tert*-butyltetrahedrane can be formed from tetra-*tert*-butylcyclobutadiene by photolysis using *n*-octane as solvent while the reverse reaction takes place thermally with an activation barrier of 26 kcal mol⁻¹¹⁶. Similarly, an *ab initio* study of the interconversion of the C₄H₄ system predicts an activation energy of about 30 kcal mol⁻¹.¹⁷ Maier and co-workers succeeded in synthesizing tetrakis (*tert*-butyl)tetrahedrane by photochemical isomerization of the corresponding cyclobutadiene.⁸ The reason for its stability is attributed to the voluminous *t*Bu-substituents that avoid the tetrahedrane skeleton from ring-opening due to the van der Waals strain among them, the so-called “corset effect”. However, this effect is lost if one of the *tert*-butyl substituents is replaced with a smaller group. Indeed, phenyl- and methyl-substituted tetrahedrane derivatives were not detected, even under matrix isolation conditions.¹⁸

Recently, it was synthesized the tetrakis (trimethylsilyl) tetrahedrane ((Me₃Si)₄THD) by photochemical isomerization of the corresponding cyclobutadiene ((Me₃Si)₄CBD),^{19,20} where (Me₃Si)₄THD

has enhanced thermal stability due the four σ -donating trimethylsilyl groups that electronically stabilize the highly strained tetrahedrane skeleton.^{21,22} Indeed, it was also reported the synthesis of perfluoroaryltetrahedranes with extended σ - π conjugation between the strained tetrahedrane core and the aromatic ring.²³ In addition, the insertion of a heteroatom (N, O, S, Ge, Si or a halogen atom) into the tetrahedrane core would be interesting because the tetrahedrane σ framework has the potential to interact with the nonbonding orbitals on the heteroatom, according to molecular orbital theory. However, such heteroatom-substituted tetrahedrane derivatives have remained elusive because of the synthetic difficulty in preparing such molecules.²⁴

In this work tetrahedrane and its derivatives were studied from different tools such as theory of density functional (DFT), quantum theory of atoms in molecules (QTAIM), atom-centered density matrix propagation (ADMP) and generalized valence bond (GVB) in order to investigate their electronic structures, thermochemical and dynamical stabilities that eventually lead to the substituents that enhance the stability of tetrahedrane cage. The results from QTAIM, GVB and the aromaticity indices provided new and important information about the main structural and electronic effects associated with the tetrahedrane cage instability and the reasons why some substituents increase its stability. Moreover, this paper also provides information about the stability of cages containing germanium and silicon parents of tetrahedrane and tetrakis(trifluoromethyl) tetrahedrane.

2. Computational details

The geometries of the studied species were optimized by using standard techniques.²⁵ Frequency calculations were performed to analyze vibrational modes of the optimized geometry in order to determine whether the resulting geometries are true minima or transition states. Calculations were performed at ω B97XD/6-311++G(d,p)²⁶ level of theory by using Gaussian 09 package,²⁷ including the electronic density which was further used for QTAIM calculations. ω B97XD functional incorporates an empirical dispersion term (D) that improves treatment of non-covalent complexes, it uses 100% Hartree Fock (HF) exchange for long-range interactions and it has an adjustable parameter (X) to include short-range exact exchange.^{28,29} Mohan and co-workers³⁰ have shown that ω B97XD functional exhibited better performance in the description of bonded and nonbonded interactions in comparison with other DFT methods. All topological information^{31,32} were calculated by means of AIM2000 software.³³ The algorithm of AIM2000 for searching critical points is based on Newton-Raphson method which relies heavily on the chosen starting point.³⁴ Integrations of the atomic basins were calculated in natural coordinates with default options of integration.

The valence bond package VB2000³⁵, version 2.5, was used for all generalized valence bond, GVB, calculations. The GVB singly occupied orbitals were calculated from VB/6-31G level theory and they were generated by means of Molekel visualization program.³⁶ The package VB2000 generates nonorthogonal

singly occupied orbitals from a general implementation of group function theory (GFT)³⁷ and modern VB methods based on high efficiency of the algebrant algorithm.^{35,38}

Nucleus Independent Chemical Shift (NICS)³⁹ and Density, Degeneracy, Delocalization-Based Index Aromaticity (D3BIA)⁴⁰ were applied to determine the aromaticity in tetrahedrane and its derivatives. D3BIA is based on density of (homo)aromatic ring, degeneracy and uniformity of the electron density among the atoms of the aromatic ring. We will use the same D3BIA formula for homoaromatic species⁴¹ where the electron density is associated with the charge density of the ring critical point (for 3c-2e bonding systems, for example) or of the cage critical point (for tridimensional 4c-2e bonding system). The degeneracy (δ) is associated with the atomic energy of the constituent atoms of the aromatic ring of the molecular system. Another important electronic feature in D3BIA is the uniformity of the electronic density calculated from the delocalization index of atoms of the aromatic ring. Then, D3BIA for homoaromatic species is defined as:

$$D3BIA = \rho(3,+3) \cdot DIU \cdot \delta \quad (1)$$

Where ρ is the ring density factor of the cage critical point (3,+3), for cage structures, and δ is the degree of degeneracy where its maximum value ($\delta=1$) is given when the difference of energy between the atoms of the cage is less than 0.009 au. The formula of δ is given in Eq. (2).

$$\delta = \frac{n}{N} \quad (2)$$

Where n is the number of atoms whose $\Delta E(\Omega) \leq 0.009au.$ and N is the total number of atoms in the homoaromatic circuit. The minimum value for n is 1, where there is no atomic pair whose $\Delta E(\Omega) \leq 0.009au.$

The DIU is the delocalization index uniformity among bridged atoms given by Eq. (3):

$$DIU = 100 - \frac{100\sigma}{\overline{DI}} \quad (3)$$

Where σ is mean deviation and \overline{DI} is the average of delocalization index between C-C, Si-Si or Ge-Ge bonds of the cage. The DI gives the amount of electron(s) between any atomic pair.³¹

The NICS values were calculated with the B3LYP/6-311++G(d,p) through the gauge-independent atomic orbital (GIAO) method⁴² implemented in Gaussian 09. The magnetic shielding tensor was calculated for ghost atoms located at the geometric center of the cage.

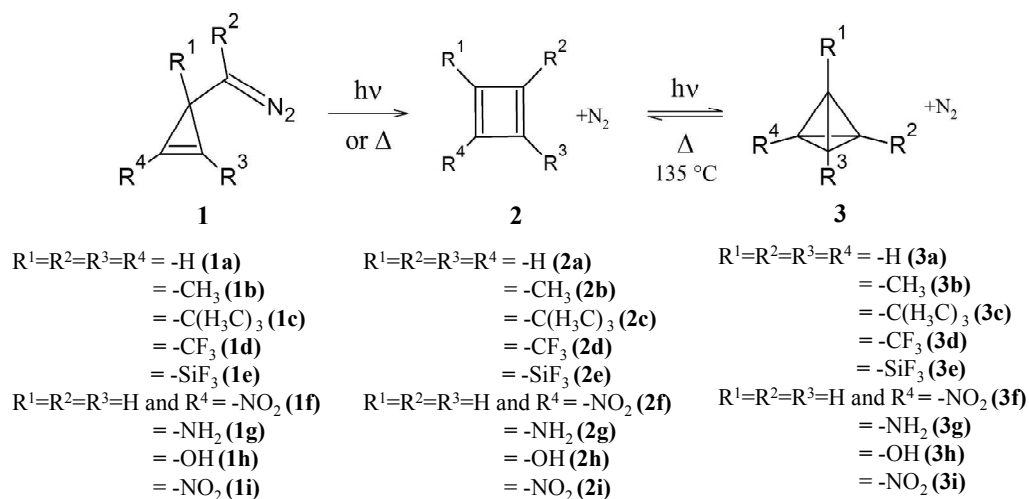
The ab initio molecular dynamics simulations involves quantum chemistry calculations aiming to obtain the potential energy and nuclear forces.⁴³⁻⁴⁶ The simulations performed in this work involved the atom-centered density matrix propagation (ADMP)⁴⁷⁻⁵⁰ in order to study the stability of tetrahedrane and

selected substituted tetrahedranes. The ADMP calculations were performed at B3LYP/6-31G(d) level of theory in Gaussian 09. A time step of 0.1 fs was used for the ADMP trajectories. The Nosé-Hoover thermostat^{51,52} was employed to maintain a constant temperature at 298.15K. The default fictitious electron mass was 0.1 amu. A maximum number of 50 steps were used in each trajectory.

3. Results and discussion

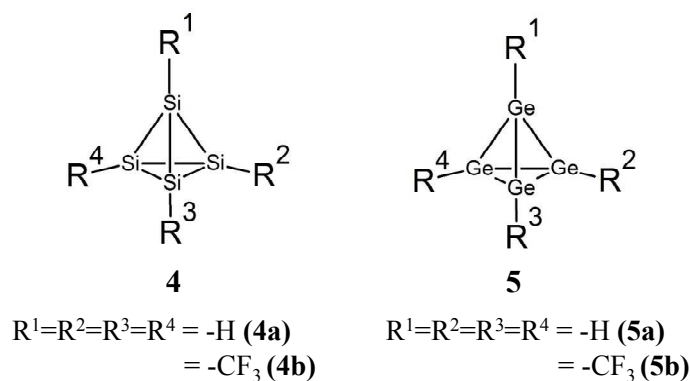
Scheme 1 shows the reaction route (diazocompounds **1a-1i** → cyclobutadienes **2a-2i** → tetrahedranes **3a-3i**) to synthesize tetrahedrane (and derivatives) from its precursors diazocompound and cyclobutadiene (and derivatives).

Scheme 1



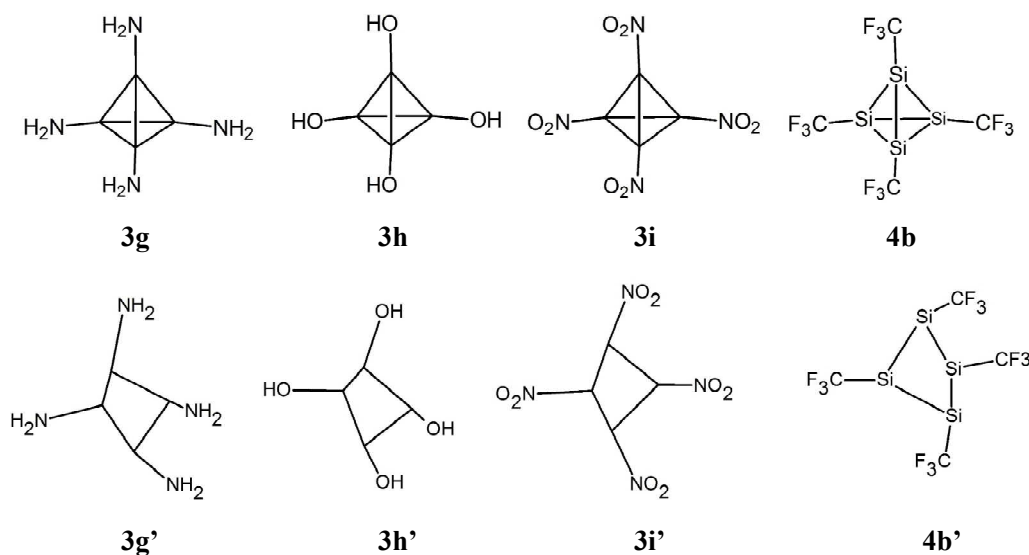
Different substituted tetrahedranes were studied: tricyclo[1.1.0.0^{2,4}]butane, **3a**, 1,2,3,4-tetramethyltricyclo[1.1.0.0^{2,4}]butane, **3b**, 1,2,3,4-tetrakis(trifluoromethyl)tricyclo[1.1.0.0^{2,4}]butane, **3c**, 1,2,3,4-tetrakis(trifluorosilyl)tricyclo[1.1.0.0^{2,4}]butane, **3d**, tetra-*tert*-butyltricyclo[1.1.0.0^{2,4}]butane, **3e**, 1-nitro tricyclo[1.1.0.0^{2,4}]butane, **3f**, 1,2,3,4-tetraamino tricyclo[1.1.0.0^{2,4}]butane, **3g**, 1,2,3,4-tetrahydroxy tricyclo[1.1.0.0^{2,4}]butane, **3h**, and 1,2,3,4-tetranitro tricyclo[1.1.0.0^{2,4}]butane, **3i**. In addition, Ge₄ and Si₄ parents of tetrahedrane, **4a-4b**, and tetrakis(trifluoromethyl) tetrahedrane, **5a-5b**, were also studied (Scheme 2).

Scheme 2



In scheme 3 shows the structures of tetraamino-substituted tetrahedrane, **3g**, tetrahydroxi-substituted tetrahedrane, **3h**, tetranitro-substituted tetrahedrane, **3i**, and tetratrimethyl-substituted silicon parent of tetrahedrane, **4b**, that were optimized and yielded the corresponding open structures **3g'**, **3h'**, **3i'** and **4b'**, which prevented any structural study with these molecules.

Scheme 3



The Scheme 3 indicates that **3g**, **3h**, **3i** and **4b** do not have stable tetrahedrane cage. However, no unique pattern can be established to account for this fact. The $-NH_2$ and $-OH$ groups are electron withdrawing groups (EWG) by inductive effect and electron donating groups (EDG) by resonance effect. On the other hand, the $-NO_2$ and $-CF_3$ do not have dual behavior and they are EWGs. Moreover, for tetrahedrane cage four $-CF_3$ do not disrupt the tetrahedrane cage while four $-NO_2$ groups do so. Conversely, in Si_4 tetrahedrane parent, $-CF_3$ disrupts the corresponding cage.

The equilibrium geometries and selected bond lengths, in Angstroms, of tetrahedrane and derivatives are depicted in Figure 1. The corresponding virial graphs are shown in Figure 2, along with several topological data of selected bond critical points. Electronic density, $\rho(\mathbf{r})$, Laplacian of the electron density, $\nabla^2 \rho(\mathbf{r})$, local energy density, $H(r)$ and relative kinetic energy density, $G(r)/\rho$ values are shown for critical points cage-substituent and electronic density, $\rho(\mathbf{r})$, Laplacian of the electron density, $\nabla^2 \rho(\mathbf{r})$, local energy density, $H(r)$, relative kinetic energy density, $G(r)/\rho$, delocalization index, DI, bond order, n , and ellipticity are shown for critical points of carbon, silicon or germanium atoms in the tetrahedrane (or parent) cage. From Figure 1, we can see that the alkyl and silyl groups impart the shortening of C-C bonds from the cage while the $-\text{CF}_3$ and $-\text{NO}_2$ groups lengthen the corresponding C-C bonds. As a consequence, based only on geometrical information, we can assume that alkyl and silyl groups behave as EWGs. These EWGs and EDGs do not disrupt the tetrahedrane cage.

We have analyzed the topology of the electron density of all species using the quantum theory of atoms in molecules (QTAIM).^{31,53,54} According to the topological analysis of QTAIM, when ρ of the critical point is relatively high ($\times 10^{-1}$ au.) and $\nabla^2 \rho < 0$, the chemical interaction is defined as shared shell and it is applied to covalent bond. However, other parameters are required to describe the nature of the chemical interaction such as the local energy density, $H(r)$, which is the sum of local kinetic energy density, $G(r)$, and local potential energy density, $V(r)$, respectively, and the ratio $G(r)/\rho$. Cremer and Kraka⁵⁵ suggested that $H(r) < 0$ and $G(r)/\rho < 1$ are indicative of shared shell (or covalent) interaction. In Figure 2 the values of ρ , $\nabla^2 \rho$, $H(r)$ and $G(r)/\rho$ of C-C, Si-Si and Ge-Ge bonds of the tetrahedrane cage (or parent) indicate that all C-C, Si-Si and Ge-Ge bond paths are shared shell interactions for **3a** – **3f**, **4a**, **5a** and **5b**. The ellipticity (ϵ) values in the tetrahedranes indicate no cylindric symmetry on the single C-C bond, while for Si-Si and Ge-Ge cages the ϵ is closer to zero indicating symmetry around the distribution of electronic density of these bonds.

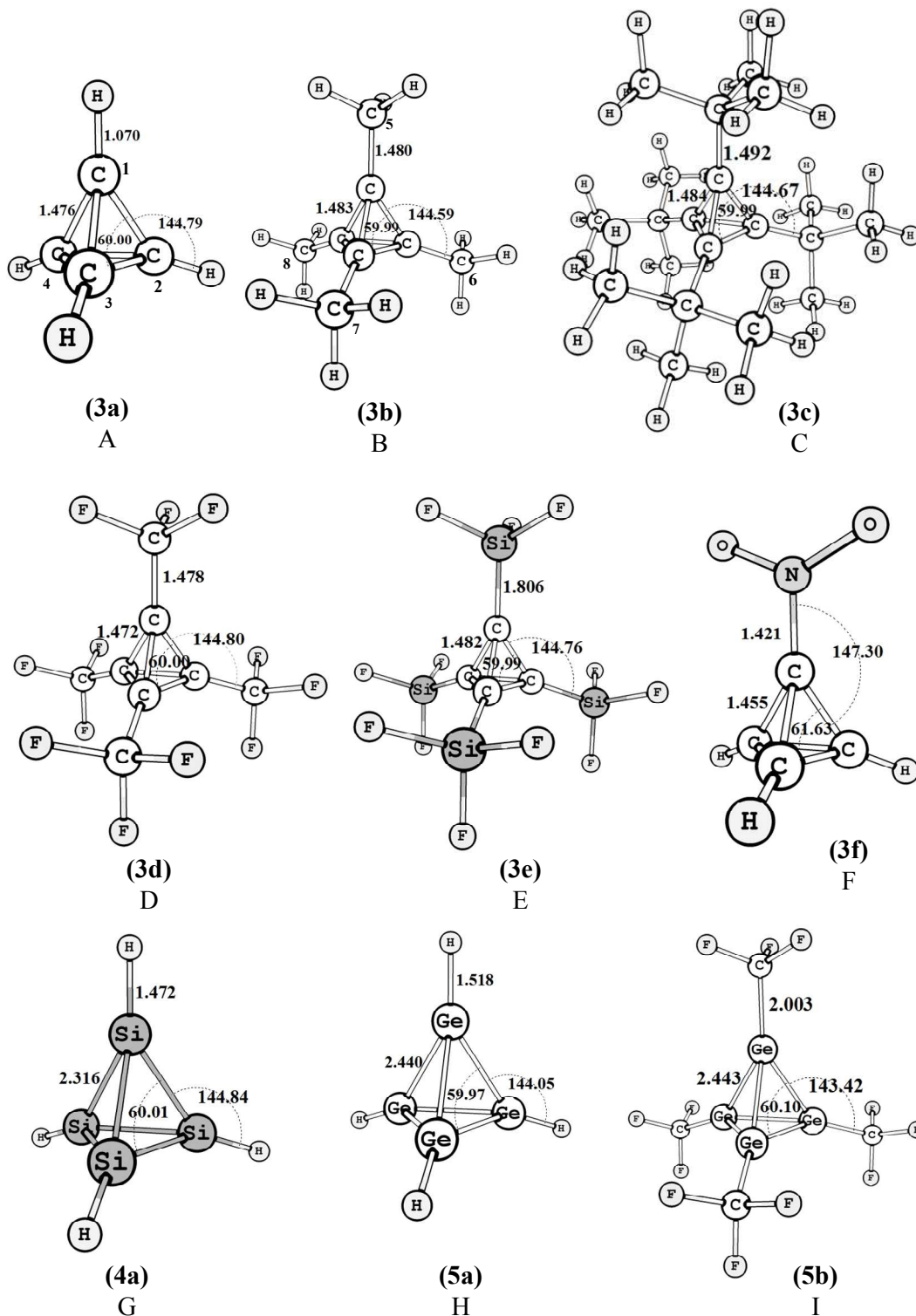


Figure 1: Optimized geometries of the substituted tetrahedranes (A-F), silicon and germanium cages (G-I) with corresponding C₁-C₄, C₁-C₅, C₁-Si, C₁-N, Si-Si, Si-H, Ge-Ge, Ge-H and Ge-C bond lengths (in Angstroms); values of selected angles (in degree).

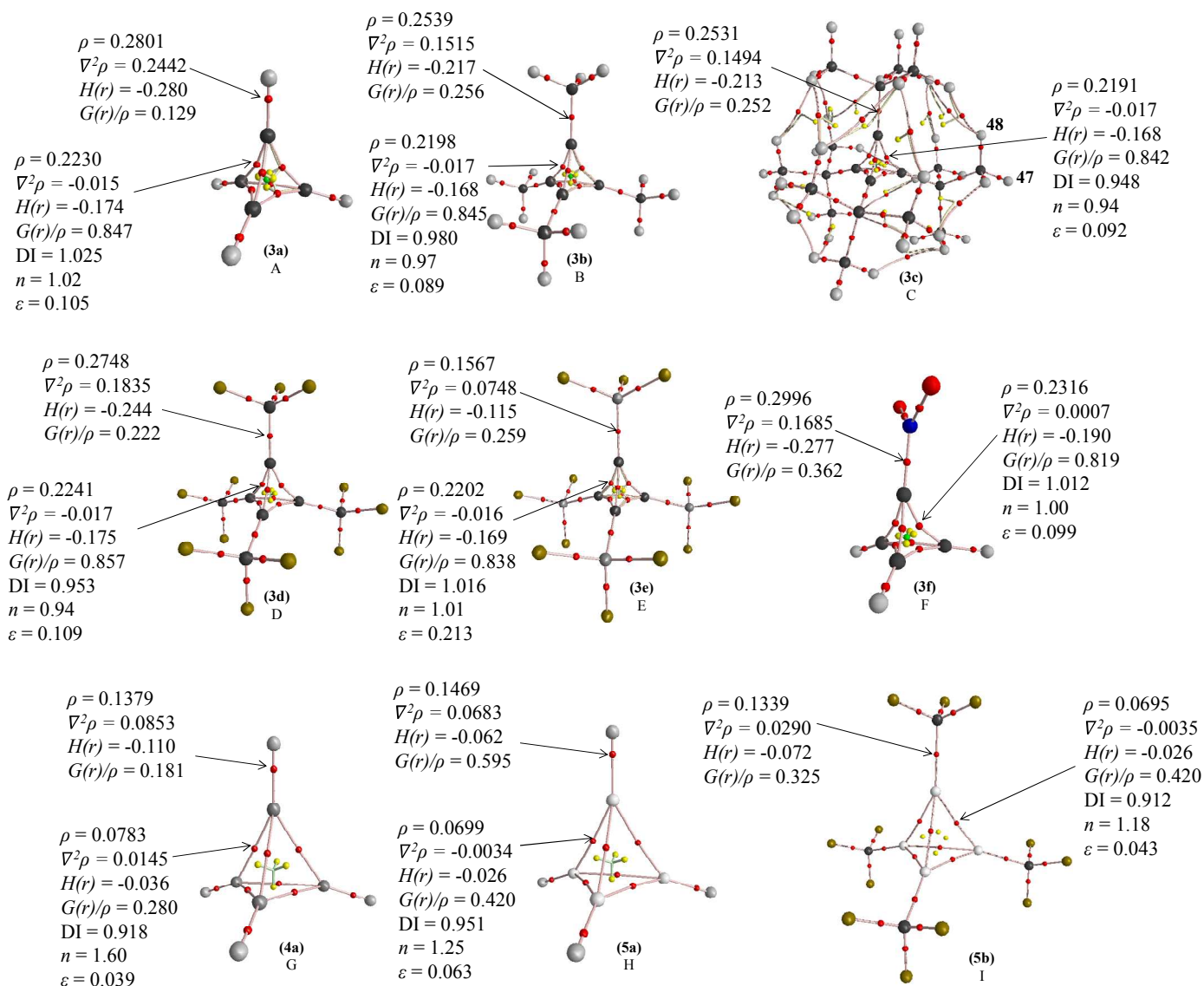


Figure 2: Virial graphs of substituted tetrahedranes (A-F), silicon and germanium cages (G-I) with the electronic density, $\rho(\mathbf{r})$, Laplacian of the electron density, $\nabla^2\rho(\mathbf{r})$, local energy density, $H(r)$ and relative kinetic energy density, $G(r)/\rho$ at cage-substituent bond critical, in au. Values of electronic density, $\rho(\mathbf{r})$, Laplacian of the electron density, $\nabla^2\rho(\mathbf{r})$, local energy density, $H(r)$, relative kinetic energy density, $G(r)/\rho$, delocalization index, DI, bond order, n , and ellipticity, ε , from carbon, silicon or germanium atoms in the tetrahedrane (or parent) cage for **3a – 3f**, **4a**, **5a** and **5b**.

The virial graph of tetra-*tert*-butyltetrahedrane, **3c**, in Figure 2C indicates a different reason for its stability rather than the so-called “corset effect” which is a steric repulsion between bulk substituents preventing the breaking of the cage.⁸ There are 23 intramolecular hydrogen-hydrogen (H-H) bonds between *tert*-butyl groups according to the virial graph of **3c** where the average charge density of the corresponding critical point, ρ_{H-H} , is 0.0041 au. The augmented cooperative effect of these small interactions contributes for

the stabilization of the molecular system.⁵⁶ An important study based on QTAIM, ELF and *ab initio* calculations demonstrated the stability effect of the H-H bonds in alkane complexes and highly branched alkanes.⁵⁷ As to the derivative **3c**, according to the values of the hydrogen atomic energy belonging or not to H-H bond, the hydrogens atoms belonging to H-H bond (e.g., H48 in Figure 2C) are in average 2.65 kcal mol⁻¹ lower in energy than those not belonging to H-H bond (e.g., H47 in Figure 1C). This result shows the stability effect of H-H bond in **3c**.

Figure 3 shows the Gibbs free energy difference along the coordination reaction from diazo compound (as a reference) to cyclobutadiene and to tetrahedrane structures (plus nitrogen), as depicted in Scheme 1.

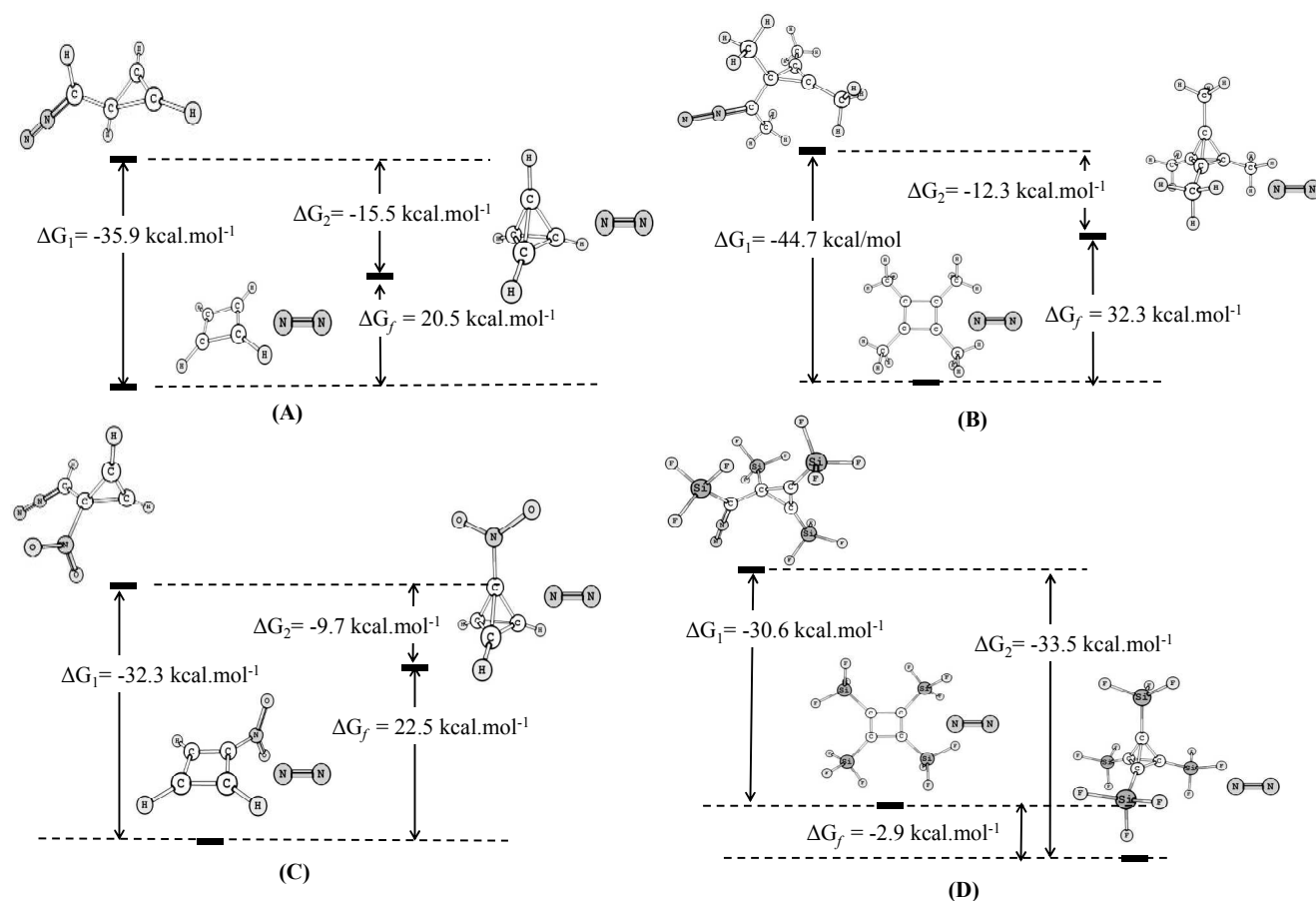


Figure 3: Gibbs free energy difference, in kcal mol⁻¹, from diazo compound (as a reference) to cyclobutadiene and tetrahedrane structures, along with nitrogen, with respect to the syntheses of **3a** (A), **3b** (B), **3f** (C) and **3e** (D).

Data of ΔG_1 in Figure 3 indicate that the diazo compounds **1a**, **1b**, **1f** and **1e** are higher in Gibbs free energy than the corresponding cyclobutadiene (or cyclobutadiene derivative), **2a**, **2b**, **2f** and **2e**, respectively. Their corresponding formation enthalpy (ΔH_1) follows the same trend (Table 1). In fact, all cyclobutadiene derivatives (**2a – 2f**), plus nitrogen molecule, are more stable than the corresponding diazo compound (Table 1). The same trend is shown for predecessors of silicon tetrahedrane parent **4a**, but nothing can be said about

the predecessors of germanium tetraedrane parents **5a** and **5b** because their corresponding diazocompounds were not formed. Likewise, the tetrahedrane and all tetrahedrane derivatives, **3a** – **3f**, are lower in energy (both enthalpy and Gibbs free energy) than the corresponding diazocompound, as indicated by ΔG_2 and ΔH_2 , except for ΔH_2 related to **3f**. The silicon tetrahedrane parent **4a** exhibits the same behavior.

Table 1 depicts the values of Gibbs free energy difference and enthalpy difference from diazocompound to cyclobutadiene (and derivatives), ΔG_1 and ΔH_1 , from diazocompound to tetrahedrane (and derivatives), ΔG_2 and ΔH_2 , and from cyclobutadiene (and derivatives) to tetrahedrane (and derivatives), ΔG_f and ΔH_f , in kcal mol⁻¹, respectively. Table 1 also shows the delocalization index, DI, bond order, n , and ellipticity, ϵ , of carbon-carbon, silicon-silicon or germanium-germanium bond in the tetrahedrane (or parent) cage, besides the bond path angle, in degree, in the tetrahedrane (or parent) cage for **3a** – **3f**, **4a**, **5a** and **5b**. The values of n were obtained from the linear relation between formal bond order (n) and delocalization index,⁵⁸ which yields very good correlations for carbon-carbon and germanium-germanium bonds, but presents moderate correlation for Si-Si bond. The ellipticity, ϵ , of a bond critical point indicate whether the corresponding bond has elliptical symmetry (when $\epsilon=0$, for single or triple bonds) or not.³¹

Table 1: Values of Gibbs free energy difference and enthalpy difference for the corresponding tetrahedranes **3a** – **3f**, **4a**, **5a** and **5b** from diazocompound to cyclobutadiene (and derivatives), ΔG_1 and ΔH_1 , from diazocompound to tetrahedrane (and derivatives), ΔG_2 and ΔH_2 , and from cyclobutadiene (and derivatives) to tetrahedrane (and derivatives), ΔG_f and ΔH_f , in kcal mol⁻¹, respectively. Values of delocalization index, DI, bond order, n , and ellipticity, ϵ , from carbon, silicon or germanium atoms in the tetrahedrane (or parent) cage, bond path angle, in degree, from bonds in the tetrahedrane (or parent) cage for **3a** – **3f**, **4a**, **5a** and **5b**.

Molecule	$\Delta G_1 /$ kcal mol ⁻¹	$\Delta G_2 /$ kcal mol ⁻¹	$\Delta H_1 /$ kcal mol ⁻¹	$\Delta H_2 /$ kcal mol ⁻¹	$\Delta G_f /$ kcal mol ⁻¹	$\Delta H_f /$ kcal mol ⁻¹	DI / e	n	ϵ	Bond path angle/ ^o
3a	-35.92	-15.45	-27.43	-6.24	20.47	21.19	1.025	1.02	0.105	76.9
3b	-44.65	-12.30	-33.77	-2.31	32.35	31.46	0.980	0.97	0.089	79.1
3c	-12.26	-27.72	-2.90	-16.48	-15.46	-13.58	0.948	0.94	0.092	78.8
3d	-37.51	-15.81	-27.04	-5.50	21.70	21.54	0.953	0.94	0.109	78.6
3e	-30.59	-33.48	-20.97	-22.71	-2.89	-1.74	1.016	1.01	0.213	72.2
3f	-32.28	-9.72	-20.76	3.45	22.55	24.21	1.012 ^(b)	1.00 ^(b)	0.099 ^(b)	80.2 ^(c)
4^a	-10.27	-8.92	-4.88	-1.11	1.35	3.77	0.918	1.60	0.039	80.6
5^a	_(a)	_(a)	_(a)	_(a)	7.24	10.60	0.951	1.25	0.063	74.0

5b _(a) _(a) _(a) _(a) -3.23 11.24 0.912 1.18 0.043 75.3

(a) The diazocompound was not obtained.

(b) Values from carbon(from cage)-nitrogen(from nitro group).

(c) Average value

Table 2 shows the topological values (AIM atomic charge, virial atomic energy, atomic volume and localization index) of the carbon, silicon and germanium atomic basins, Ω , of the tetrahedrane (or parent) cage for **3a** – **3f**, **4a**, **5a** and **5b**. These values are obtained from the integration of the corresponding atomic basin.

Table 2: Values of AIM atomic charge, $q(\Omega)$, atomic energy, $E(\Omega)$, atomic dipole moment, $M(\Omega)$, atomic volume, $V(\Omega)$ and localization index, LI of carbon, silicon and germanium atoms in tetrahedrane, silicon and germanium derivatives, respectively.

Molecule	$q(\Omega)$	$E(\Omega)$	$M(\Omega)$	$V(\Omega)$	LI
3a	-0.121	-38.0936	0.435	6.09	4.059
3b	-0.109	-38.1522	0.292	6.10	3.968
3c	-0.089	-38.1732	0.300	6.09	3.934
3d	0.037	-38.0509	0.202	6.10	3.844
3e	-0.697	-38.2994	1.48	6.69	4.732
3f	0.235 ^(a)	-37.9671 ^(a)	0.305 ^(a)	5.76 ^(a)	3.691 ^(a)
4a	0.655	-289.3407	0.889	13.30	11.44
5a	0.283	-2074.3391	0.076	31.66	29.74
5b	0.387	-2074.3590	0.097	31.57	29.66

(a) Values of carbon atom attached to the nitro group.

Despite the antiaromatic nature of cyclobutadiene or its derivatives and the σ -aromaticity¹⁰ of tetrahedrane cage, in most cases, tetrahedrane and its derivatives are higher in energy (both enthalpy and Gibbs free energy) than the corresponding cyclobutadiene as it is indicated by ΔG_f and ΔH_f . The fact that the σ -aromaticity¹⁰ of tetrahedrane (or derivatives) does not impart smaller energy in comparison to the corresponding cyclobutadiene (which is antiaromatic) can be attributed to the highly strained cage structure of tetrahedrane and derivatives, except for **3c** and **3e** which are more stable than **2c** and **2e**. As for **3c**, QTAIM analysis indicates that its relative stability is ascribed to a large amount of stabilizing hydrogen-hydrogen bonds, as aforementioned, while the relative stability of **3e** is possibly reasoned by the great

charge density donator effect of the $-\text{SiF}_3$ group, according to the more negative values of $q(\text{C})$ and $E(\text{C})$ plus higher values of $V(\text{C})$ and $\text{LI}(\text{C})$ compared to those from **3a**. Nonetheless, the relative stability imparted by hydrogen-hydrogen bond in **3c** is nearly 12 kcal mol^{-1} higher than that bestowed by the donation effect of $-\text{SiF}_3$ group in **3e**.

Taking values of any topological property of tetrahedrane **3a** as a reference, the DI values of C-C bonds in the tetrahedrane cage of **3e** indicates that trifluorosilyl group partially removes the charge density of each C-C bond (Table 1 and Figure 2) where $\rho = 0.2801 \text{ u.a.}$ and 0.2539 u.a. for **3a** and **3e** respectively. However, from Table 2, the AIM atomic charge of carbon atom in **3e** is 6 times more negatively charged than that from **3a**, which is corroborated by a greater localization index and greater atomic volume of carbon atom in **3e**. In addition, the virial atomic energy of each carbon atom in **3e** is 0.2058 au. smaller than that from **3a**. Then, $-\text{SiF}_3$ pronouncedly donates charge density to the carbon atoms of the tetrahedrane cage in **3e**, although removes partially the charge density in the C-C bonding region. There is also a greater atomic dipole moment in the carbon atoms of **3e** in comparison with those from all other studied tetrahedrane derivatives or parents, which can be partially related to a larger amount of charge density within carbon atomic basins in **3e**, besides the influence of the electropositive $\text{Si}(\text{F}_3)$ atom bonded to the carbon atom. Then, $-\text{SiF}_3$ in **3e** increases the charge density of C atom attached to it but removes the charge density of the adjacent C-C bond.

Conversely, the methyl and *t*-butyl groups, in **3b** and **3c**, respectively, are probably EWGs according to carbon atomic charge and localization index, where these values are slightly less negative, than those from **3a**. Moreover, methyl and *t*-butyl groups also partially remove charge density from C-C region bond of tetrahedrane cage, as indicated by the corresponding charge density of BCP (see Figure 2B and 2C), the DI, bond order and ellipticity (see Table 1) in comparison with those values from **3a**.

The nitro group in **3f** has a more pronounced electron withdrawing effect than alkyl groups as can be easily observed in the positive atomic charge, low LI and higher atomic energy of the carbon atom attached to the nitro group in **3f** with respect to those values for the carbon atoms in **3a** (Table 2). Nonetheless, **3b** is more unstable than **3f**, but **3f** is slightly more unstable than **3a**. Then, one nitro group stabilizes the tetrahedrane cage in comparison with four methyl groups, but four hydrogen substituents (in **3a**) still generate a more stable structure than one nitro and three hydrogen substituents (in **3f**).

Figure 4 shows the doubly occupied GVB oxygen lone pair of nitro group, LP1 and LP2, and singly occupied C-C sigma orbitals, $\text{VB}(\text{C-C})'$, $\text{VB}(\text{C-C})_1$ and $\text{VB}(\text{C-C})_2$, of **3f**. Table 4 shows the overlap integrals between the GVB orbitals of Figure 4. From GVB orbitals of **3f** (Figure 4), one of the oxygen lone pair, named LP2, is directed towards the cage. The average overlap integral between LP2 and C-C bonds in the cage (LP2-CC_1) are three-fold greater than the average overlap integral between LP1 (which is not directed towards the cage) and C-C bonds in the cage (LP1-CC_1) as indicated in Table 4. Then, we can infer

that the influence of both oxygen LP2 lone pairs from four nitro groups may cause a great instability and may lead to the disruption of tetrahedrane cage in **3i** yielding **3i'**.

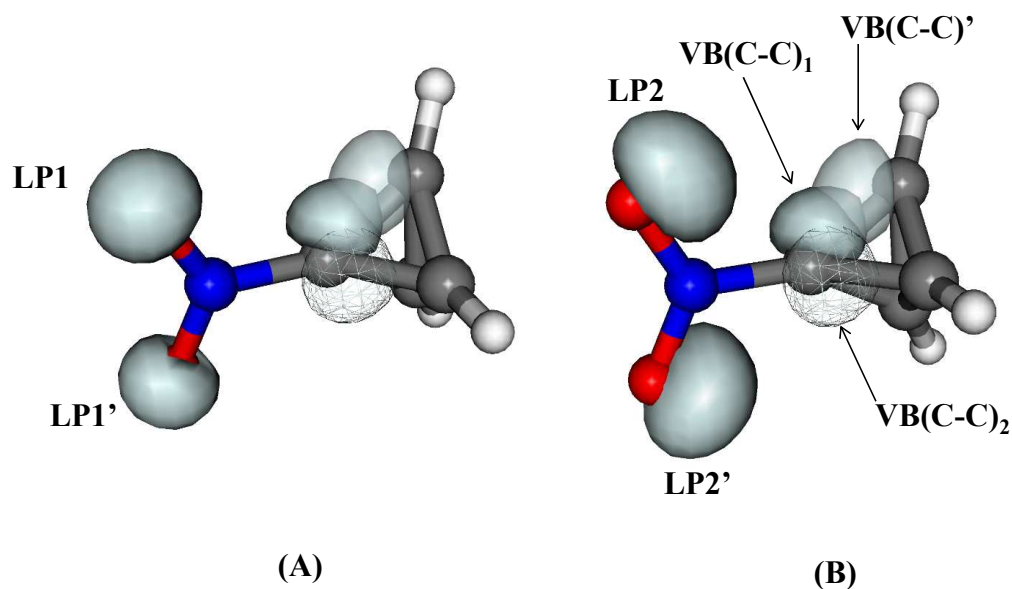


Figure 4: Doubly occupied generalized valence bond (GVB) orbitals of lone pairs of oxygen of nitro ($-\text{NO}_2$) functional group substituent (LP1, LP1', LP2 and LP2') (A and B) and singly occupied GVB orbitals of C-C sigma bond [$\text{VB}(\text{C}-\text{C})_1$, $\text{VB}(\text{C}-\text{C})_2$ and $\text{VB}(\text{C}-\text{C})'$] (B).

Table 4: Overlap matrix of selected GVB orbitals of molecule **3f** of two oxygen lone pairs (LP1, LP2, LP1' and LP2') and of two C-C sigma bonds [$\text{VB}(\text{C}-\text{C})_1$, $\text{VB}(\text{C}-\text{C})'$ and $\text{VB}(\text{C}-\text{C})_2$].

	LP1	LP1'	LP2	LP2'
$\text{VB}(\text{C}-\text{C})_1$	0.007	0.019	0.054	0.045
$\text{VB}(\text{C}-\text{C})_2$	0.005	0.005	0.005	0.006
$\text{VB}(\text{C}-\text{C})'$	0.008	0.006	0.034	0.009

When comparing topological data between **3d** and **3f** in Table 2, we observe that the trifluoromethyl group in **3d** has a less electron withdrawing effect than the nitro group in **3f**, since carbon atomic charge is less positive in **3d**, carbon atomic energy is more stable in **3d**, and LI is greater in **3d**. In addition, the $-\text{CF}_3$ group also decreases the charge density in the C-C bonding region as noted from its DI

and bond order (Table 1). In terms of molecular energy, the stability of **3d** is quite similar to that from **3a** and it is slightly higher than that from **3f**.

To sum up the energetic influence of the studied substituents in tetrahedrane cage we can note that EWGs such as $-\text{CF}_3$ do not affect the relative stability of the tetrahedrane cage, while with a stronger EWG (e.g., $-\text{NO}_2$) the tetrahedrane cage becomes slightly more unstable. On the other hand, slight EWG such as $-\text{CH}_3$ imparts a higher instability in tetrahedrane cage. Conversely, a σ -EDG such as $-\text{SiF}_3$ makes the tetrahedrane cage more stable, while a π -EDG (e.g. $-\text{NH}_2$ and $-\text{OH}$) disrupts the tetrahedrane cage. These trends can be observed in the decreasing order of ΔG_f (**3c** > **3e** > **3a** > **3d** > **3f** > **3b**) and ΔH_f (**3c** > **3e** > **3a** > **3d** > **3f** > **3b**), without the silicon and germanium parents.

The integration of the atomic basins gives the value of the bond path angle of the electron density function. The bond path angle involving the atoms in the cage of all tetrahedrane derivatives and Si/Ge parents is higher than the corresponding geometric bond angle (Table 1). The increase of the bond angle in cyclopropane ring (which is part of the tetrahedrane cage) decreases its ring strain (or cage strain) which is so-called banana bond.⁵⁹ However, there is no linear relation between bond path angle and ΔG_f for the studied series.

The tetrahedrane cage with silicon and germanium atoms, **4a** and **5a**, were also obtained, as well as trifluoromethyl tetrasubstituted germanium cage, **5b**. However, the trifluoromethyl tetrasubstituted silicon parent disrupted during optimization procedure (Scheme 3). Formation enthalpy, ΔH_f , indicates that they have intermediate stability between the most stable (**3c** and **3e**) and least stable (**3a**, **3b**, **3d** and **3f**) substituted tetrahedranes. Nonetheless, this stability order does not match the aromaticity order, according to NICS and D3BIA, where the set **4a**, **5a** and **5b** are the least aromatic.

Table 3 shows the topological values (\overline{DI} , DIU, δ and $\rho(3,+3)$) associated with the D3BIA formula for homoaromatic and cage structures, along with NICS values in the geometrical center of the tetrahedrane (or parent) cage for **3a**, **3b**, **3c**, **3d**, **3e**, **3f**, **4a**, **5a** and **5b**. The aromaticity of the substituted tetrahedranes, germanium and silicon parents were investigated with two aromaticity indices: NICS and D3BIA. Hereafter we mention the increase or decrease of NICS with respect to the aromaticity where aromaticity increases with higher negative values of NICS and decreases with lower negative values (or higher positive values) of NICS.

Figure 5 shows the linear relations between NICS and D3BIA where Figure 5A lacks only one molecule, **3f**, and Figure 5B has all the studied molecules (**3a-3f**, **4a**, **4b** and **5a**).

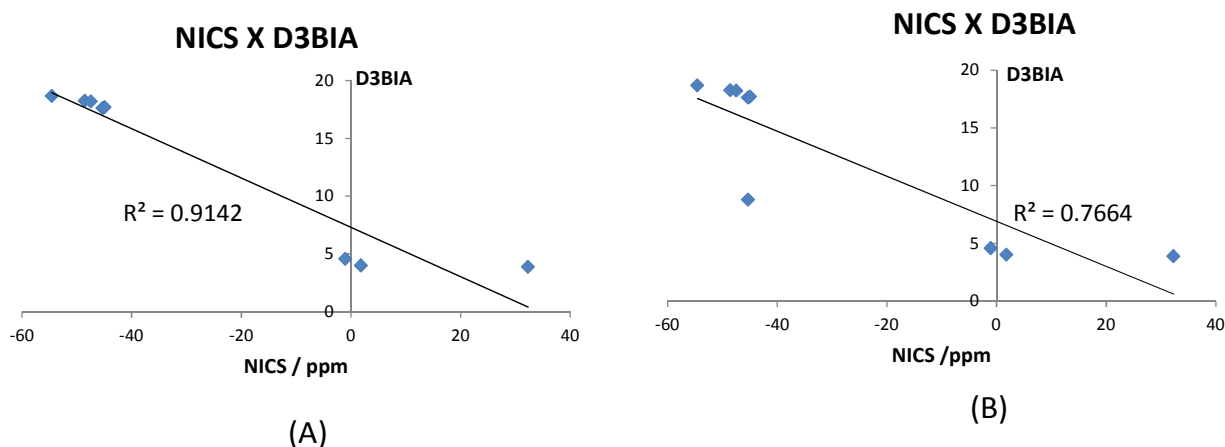


Figure 5: (A) Plot of NICS versus D3BIA for **3a-3e**, **4a**, **4b** and **5a**; (B) Plot of NICS versus D3BIA for **3a-3f**, **4a**, **4b** and **5a**.

Figure 5A shows a very good linear relation between NICS and D3BIA where **3f** was excluded because NICS in **3f** is higher (more negative) than it is supposed to be since **3c** is $10.81 \text{ kcal mol}^{-1}$ more stable than **3f** but they have the same NICS value. Probably, this is the influence of lone pairs of oxygen atoms from nitro group that interact with the tetrahedrane cage of **3f** (Figure 4 and Table 4) which enhances its NICS value.

Table 3: Average DI, \overline{DI} , of the carbon or silicon or germanium atoms in the tetrahedrane (or parent) cage, the corresponding DIUs, the degree of degeneracy (δ) involving the atoms of the tetrahedrane (or parent) cage, the charge density of the cage critical points [$\rho(3,+3)$], D3BIA and NICS values for **3a**, **3b**, **3c**, **3d**, **3e**, **3f**, **4a**, **5a** and **5b**.

Molecule	\overline{DI}	DIU	δ	$\rho(3,+3)/\text{au}$	D3BIA	NICS / ppm
3a	1.025	99.97	1.0	0.182	18.24	-48.53
3b	0.979	99.89	1.0	0.176	17.61	-45.31
3c	0.954	99.99	1.0	0.177	17.68	-44.95
3d	0.961	99.98	1.0	0.182	18.21	-47.45
3e	1.029	99.97	1.0	0.187	18.67	-54.54
3f	0.997	96.77	0.5	0.181	8.77	-45.30
4a	0.933	99.95	1.0	0.046	4.57	-1.03
5a	0.951	99.99	1.0	0.040	4.00	1.85

5b	0.911	99.93	1.0	0.039	3.88	32.33
-----------	-------	-------	-----	-------	------	-------

The alkyl groups (in **3b** and **3c**) decrease both NICS and D3BIA in comparison with **3a**. Likewise, the trifluoromethyl and nitro groups in **3d** and **3f**, respectively, also decrease both aromaticity indices with respect to **3a**. On the other hand, the trifluorosilyl group increases both NICS and D3BIA in **3e**. Then, we may assume that EWGs decrease the aromaticity of the tetrahedrane cage while the EDG increases its aromaticity. The decreasing order of formation enthalpy and NICS for **3a-3f** is nearly the same (except for **3c** where hydrogen-hydrogen bonds play an important role on its stabilization): **3e** > **3a** > **3d** > **3b** \cong **3f** (for NICS) and **3e** > **3a** > **3d** > **3f** > **3b** (for ΔH_f). Then, we may assume that the aromaticity (influenced by EWGs or EDGs) is an important stability factor in the tetrahedrane cage besides the intramolecular hydrogen-hydrogen bonds in **3c**.

As aforementioned, regarding the set **4a**, **5a** and **5b**, there is no relation between their stability and aromaticity orders. According to NICS, they are not aromatic molecules, but their stability is higher than that in **3a**, **3b**, **3d** and **3f**. Probably, the stabilities of **4a**, **5a** and **5b** are influenced by their predecessors' stabilities. Regarding **4a**, its ΔH_1 is the least negative, which means that its corresponding silicon cyclobutadiene parent is the least stable of all set of substituted cyclobutadienes. Then, the high instability of predecessor of **4a** plays an important role on the large relative stability of **4a**.

Figure 6 shows the singly occupied GVB orbitals of sigma C-C bonds, VB(C-C)', VB (C-C)₁ and VB (C-C)₂, of **3a**, **3b**, **3f** and cubane. Table 5 shows the overlap integral between the singly occupied GVB orbitals represented in Figure 6. Tetrahedrane and cubane are platonic hydrocarbons where only cubane was synthetically obtained.⁶⁰ The overlap between vicinal GVB orbitals in cubane, VB(C-C)₁ – VB(C-C)₂, is 0.224 – nearly four times smaller than the overlap between GVB orbitals of each C-C bond, VB (C-C)₁ – VB(C-C)'. The overlap between vicinal GVB orbitals in tetrahedrane is higher than that from cubane, 0.279, where we can infer that vicinal C-C bonds tend to increase the electronic repulsion in the tetrahedrane cage, which could partially explain the instability of tetrahedrane with respect to cubane. The electron withdrawing effect of alkyl group can also be noticed by the slightly smaller overlap between vicinal GVB orbitals in **3b** (Table 5). Likewise, the higher electron withdrawing effect of the nitro group can also be noticed from overlap of GVB orbital because this value in **3f** is similar to that from cubane. However, as aforementioned **3b** **3f** is more unstable than **3a**. Then, the electronic repulsion from vicinal C-C bonds within the cage is not the main instability factor of tetrahedrane cage which means that the main reason for tetrahedrane instability should be attributed to its angle strain.

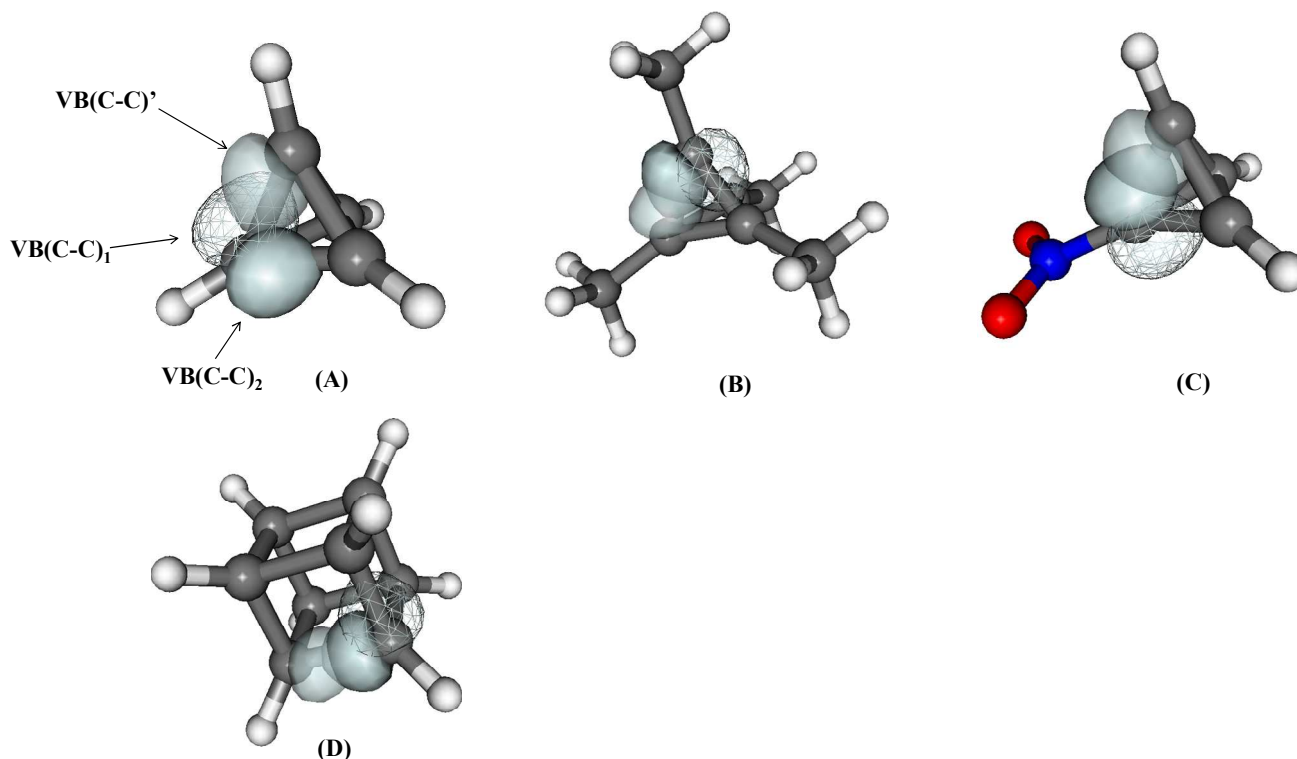


Figure 6: Singly occupied generalized valence bond (GVB) orbitals of C-C sigma bond [VB(C-C)₁, VB(C-C)₂ and VB(C-C)'] of **3a** (A), **3b** (B), **3f** (C) and cubane (D).

Table 5: Overlap matrix of selected GVB orbitals, VB(C-C)', VB (C-C)₁ and VB (C-C)₂, of **3a**, **3b**, **3f** and cubane.

	VB(C-C) ₁			
	3a	3b	3f	Cubane
VB(C-C) ₂	0.279	0.272	0.224	0.224
VB(C-C)'	0.828	0.826	0.823	0.810

^aVB orbitals of **3a**

^bVB orbitals of **3b**

^cVB orbitals of **3f**

^dVB orbitals of cubane

The Figures 7, 8 and 9 shows the plots of total energy (in Hartree) versus the time of trajectory of 5 fs using atom-centered density matrix propagation (ADMP) method for tetrahedrane and substituted tetrahedranes (**3a**, **3c** and **3e**) where the starting structure was previously optimized at ω B97XD/6-311++G(d,p) level of theory. We used ADMP calculations to test the stability of selected tetrahedrane cages under dynamic simulation. Some corresponding structures from selected points of each trajectory are also

depicted in Figures 7, 8 and 9. In Figure 7, we can see that no significant changes occur in **3a** structure at the beginning of the trajectory (0.2 to 0.6 fs). However, at about 1.3 fs the C2-H7 bond is broken. At 2.8 fs the C3-H5 bond is broken and C4-H8 bond length increases. Moreover, the C-C bond lengths of three cyclopropane rings of tetrahedrane cage shorten. At about 4.2 fs, the C4-H8 bond is broken and at 5.0 fs the C3-H5 bond is restored. Then, during the ADMP trajectory, **3a** undergoes structural changes in its structure but it is not restored to its starting optimized geometry at any point. On the other hand, there is no significant change in the total energy of **3c** during the course of its trajectory (Figure 8). Then, **3c** has a thermochemical and dynamical relative stability mainly due to the large amount of stabilizing H-H bonds. Likewise, **3e** presented a similar behavior (Figure 9), but its relative stability is given by $-\text{SiF}_3$ group that acts as σ -EDG, where in 2.5 fs and 4.4 fs occurs a decreasing in two C-Si bond lengths (indicated by red arrows) according to the nature of donating electrons of trifluorosilyl group.

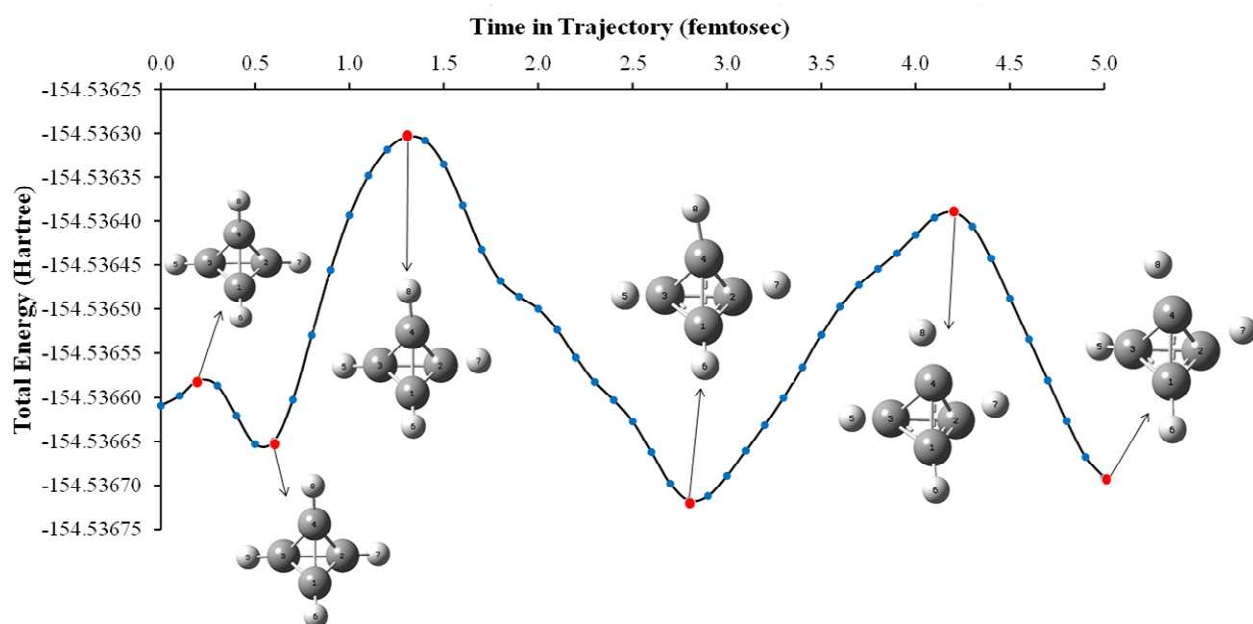


Figure 7: Plot of total energy, in Hartree, versus the time of trajectory, in femtoseconds, of tetrahedrane (**3a**) using ADMP method. Some structures are depicted at the corresponding selected points of the trajectory.

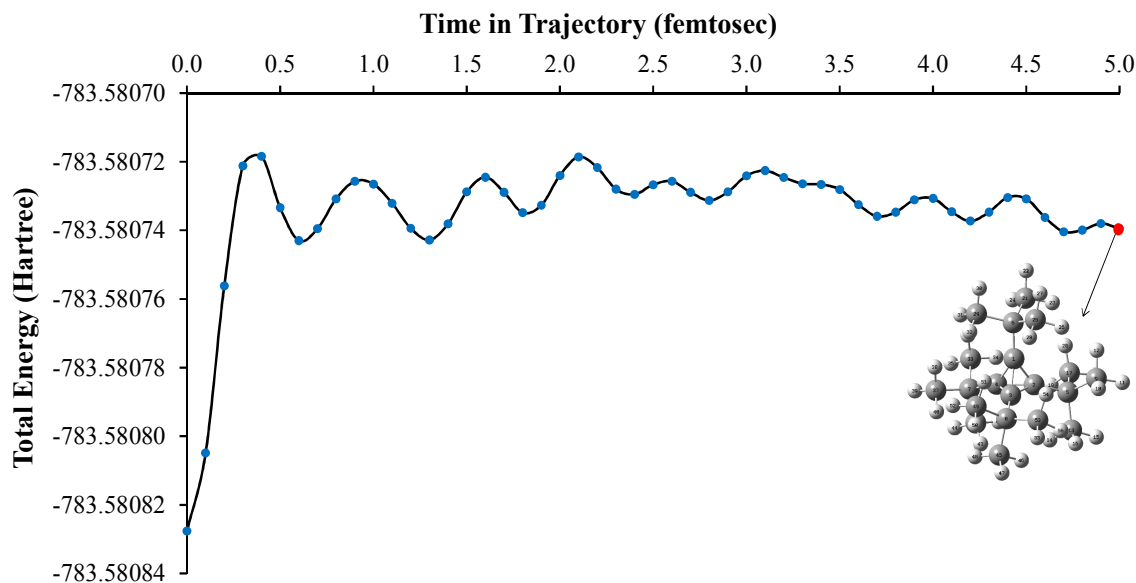


Figure 8: Plot of total energy, in Hartree, versus the time of trajectory, in femtoseconds, of **3c** using ADMP method. The structure at the end of trajectory is also depicted

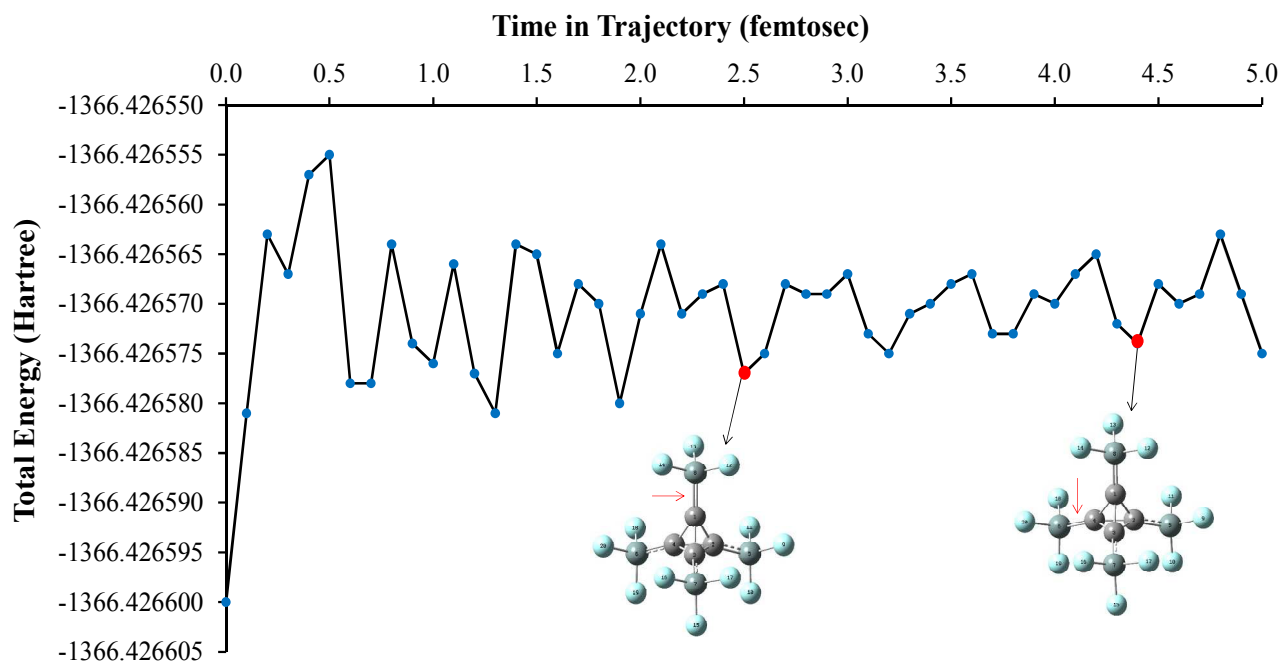


Figure 9: Plot of total energy, in Hartree, versus the time of trajectory, in femtoseconds, of **3e** using ADMP method. A couple of structures are depicted at the selected corresponding points of the trajectory.

Conclusions

The influence of substituents on the stability of the tetrahedrane cage reveals that strong electron withdrawing groups do not affect significantly the relative stability in the tetrahedrane cage, unlike weak EWG that generate a large instability in tetrahedrane cage. However, substituents that act as sigma electron donating groups (σ -EDG) stabilize the tetrahedrane cage, although π -EDGs leads to disruption of the tetrahedrane cage.

According to NICS and D3BIA and their relations with the corresponding formation enthalpy, the aromaticity is an important factor for the stability of the tetrahedrane cage. The σ -EDGs increase both aromaticity and stability of the tetrahedrane cage, whereas the EWGs decrease both aromaticity making and cage stability, except for **3c** in which its stability is due to the intramolecular hydrogen-hydrogen bonds. Although there is no relation between aromaticity and stability for germanium and silicon tetrahedrane parents **4a**, **5a** and **5b** their NICS and D3BIA values indicate that these molecules are not aromatic.

According to generalized valence bond method, one of the oxygen lone pair has an electronic repulsion with C-C bonds in its tetrahedrane cage and probably when four nitro groups are attached to the tetrahedrane cage the higher electronic repulsion may lead to disruption of corresponding substituted

tetrahedrane. Moreover, the GVB analysis indicate that the instability of the tetrahedrane cage is mainly imparted by its high strain energy while the C-C electronic repulsion within the cage has a minor influence.

The ADMP analysis indicates that tetrahedrane **3a** is dynamically unstable where some C-H bonds break during the simulation trajectory. Conversely, **3c** and **3e** remain its structure during the whole trajectory. Therefore, thermodynamic and dynamic results are in accordance for the relatively stable and unstable cage structures.

Acknowledgments

Authors thank, Fundação de Apoio à Pesquisa do Estado do Rio Grande do Norte (FAPERN), Coordenação de Ensino de Aperfeiçoamento de Pessoal de Nível Superior (CAPES) and Conselho Nacional de Desenvolvimento Científico e Tecnológico (CNPq) for financial support.

References

1. G. Zhou, J.-L. Zhang, N.-B. Wong, and A. Tian, *J. Mol. Struct. THEOCHEM*, 2004, **668**, 189–195.
2. J. P. Agrawal, *Prog. Energy Combust. Sci.*, 1998, **24**, 1–30.
3. T. J. Katz and N. Acton, *J. Am. Chem. Soc.*, 1973, **95**, 2738–2739.
4. W. G. Dauben and A. F. Cunningham, *J. Org. Chem.*, 1983, **48**, 2842–2847.
5. G. Zhou, J. Wang, W.-D. He, N.-B. Wong, A. Tian, and W.-K. Li, *J. Mol. Struct. THEOCHEM*, 2002, **589-590**, 273–280.
6. J. Zhang and H. Xiao, *J. Chem. Phys.*, 2002, **116**, 10674.
7. R. F. Peterson Jr., R. T. K. Baker, and R. L. Wolfgang, *Tetrahedron Lett.*, 1969, **10**, 4749–4752.
8. G. Maier, S. Pfriem, U. Schäfer, and R. Matusch, *Angew. Chemie Int. Ed. English*, 1978, **17**, 520–521.
9. K. B. Wiberg, R. F. W. Bader, and C. D. H. Lau, *J. Am. Chem. Soc.*, 1987, **109**, 985–1001.
10. D. Moran, M. Manoharan, T. Heine, and P. von R. Schleyer, *Org. Lett.*, 2002, **5**, 23–26.
11. S. Bally, T.; Masamune, *Angew. Chemie*, 1980, **92**, 1521–3757.
12. D. J. Cram, M. E. Tanner, and R. Thomas, *Angew. Chemie Int. Ed. English*, 1991, **30**, 1024–1027.
13. H. Irgartinger and H. Rodewald, *Angew. Chemie Int. Ed. English*, 1974, **13**, 740–741.
14. C. Hill and N. Carolina, 1973, 1973–1974.

15. H. Imgartinger, N. Riegler, K.-D. Malsch, K.-A. Schneider, and G. Maier, *Angew. Chemie*, 1980, **92**, 214–215.
16. G. Maier, *Pure Appl. Chem*, 1991, **63**, 275–282.
17. H. Kollmar, *J. Am. Chem. Soc.*, 1980, **102**, 2617–2621.
18. G. Maier, H. P. Reisenauer, and H.-A. Freitag, *Tetrahedron Lett.*, 1978, **19**, 121–124.
19. G. Maier, J. Neudert, O. Wolf, D. Pappusch, A. Sekiguchi, M. Tanaka, and T. Matsuo, *J. Am. Chem. Soc.*, 2002, **124**, 13819–26.
20. G. Maier, J. Neudert, and O. Wolf, *Communications*, 2001, 1674–1675.
21. J. D. Dill and A. Greenberg, *Notes*, 1979, 6814–6826.
22. G. Maier and D. Born, *Angew. Chemie Int. Ed. English*, 1989, **28**, 1050–1052.
23. M. Nakamoto, Y. Inagaki, M. Nishina, and A. Sekiguchi, *J. Am. Chem. Soc.*, 2009, **131**, 3172–3173.
24. T. Ochiai, M. Nakamoto, Y. Inagaki, and A. Sekiguchi, *J. Am. Chem. Soc.*, 2011, **133**, 11504–7.
25. R. Fletcher, *Practical Methods of Optimization: Unconstrained optimization*, J. Wiley, New York, 1980.
26. Y. Minenkov, A. Singstad, G. Occhipinti, and V. R. Jensen, *Dalton Trans.*, 2012, **41**, 5526–41.
27. M. J. Frisch, G. W. Trucks, H. B. Schlegel, G. E. Scuseria, M. A. Robb, J. R. Cheeseman, G. Scalmani, V. Barone, B. Mennucci, G. A. Petersson, H. Nakatsuji, M. Caricato, X. Li, H. P. Hratchian, A. F. Izmaylov, J. Bloino, G. Zheng, J. L. Sonnenberg, M. Hada, M. Ehara, K. Toyota, R. Fukuda, J. Hasegawa, M. Ishida, T. Nakajima, Y. Honda, O. Kitao, H. Nakai, T. Vreven, J. A. Montgomery, J. E. Peralta, F. Ogliaro, M. Bearpark, J. J. Heyd, E. Brothers, K. N. Kudin, V. N. Staroverov, R. Kobayashi, J. Normand, K. Raghavachari, A. Rendell, J. C. Burant, S. S. Iyengar, J. Tomasi, M. Cossi, N. Rega, J. M. Millam, M. Klene, J. E. Knox, J. B. Cross, V. Bakken, C. Adamo, J. Jaramillo, R. Gomperts, R. E. Stratmann, O. Yazyev, A. J. Austin, R. Cammi, C. Pomelli, J. W. Ochterski, R. L. Martin, K. Morokuma, V. G. Zakrzewski, G. A. Voth, P. Salvador, J. J. Dannenberg, S. Dapprich, A. D. Daniels, Farkas, J. B. Foresman, J. V Ortiz, J. Cioslowski, and D. J. Fox, *Gaussian 09, Revis. B.01, Gaussian, Inc., Wallingford CT*, 2009.
28. K. S. Thanthiriwatte, E. G. Hohenstein, L. a. Burns, and C. D. Sherrill, *J. Chem. Theory Comput.*, 2011, **7**, 88–96.
29. J. Cooper, C. Grant, and J. Zhang, *Rep. Theor. Chem*, 2012, **1**, 11–19.
30. N. Mohan, K. P. Vijayalakshmi, N. Koga, and C. H. Suresh, *J. Comput. Chem.*, 2010, **31**, 2874–82.
31. R. F. W. Bader, *Atoms in Molecules: A Quantum Theory*, Oxford University Press, USA, 1994.
32. P. Popelier, *Coord. Chem. Rev.*, 2000, **197**, 169–189.
33. F. Dijkstra and J. H. van Lenthe, *J. Comput. Chem.*, 2001, **22**, 665–672.
34. F. Biegler-König and J. Schönbohm, *J. Comput. Chem.*, 2002, **23**, 1489–1494.
35. J. Li and R. McWeeny, *Int. J. Quantum Chem.*, 2002, **89**, 208–216.

36. S. Portmann and H. P. Lüthi, *Chim. Int. J. Chem.*, 54, 766–770.
37. R. McWeeny, *Proc. R. Soc. A Math. Phys. Eng. Sci.*, 1959, **253**, 242–259.
38. J. Li and R. Pauncz, *Int. J. Quantum Chem.*, 1997, **62**, 245–259.
39. A. Stanger, *J. Org. Chem.*, 2005, **71**, 883–893.
40. C. L. Firme, S. E. Galembeck, O. A. C. Antunes, and P. M. Esteves, *J. Braz. Chem. Soc.*, 2007, **18**, 1397–1404.
41. C. L. Firme, O. A. C. Antunes, and P. M. Esteves, *J. Braz. Chem. Soc.*, 2008, **19**, 140–149.
42. J. R. Cheeseman, G. W. Trucks, T. A. Keith, and M. J. Frisch, *J. Chem. Phys.*, 1996, **104**, 5497.
43. E. Deumens, A. Diz, R. Longo, and Y. Öhrn, *Rev. Mod. Phys.*, 1994, **66**, 917–983.
44. M. Pavese, D. R. Berard, and G. A. Voth, *Chem. Phys. Lett.*, 1999, **300**, 93–98.
45. H. B. Schlegel, J. M. Millam, S. S. Iyengar, G. A. Voth, A. D. Daniels, G. E. Scuseria, and M. J. Frisch, *J. Chem. Phys.*, 2001, **114**, 9758.
46. I. S. Y. Wang and M. Karplus, *J. Am. Chem. Soc.*, 1973, **95**, 8160–8164.
47. S. Iyengar, H. Schlegel, and G. Voth, *J. Phys. ...*, 2003, **107**, 7269–7277.
48. L. Zhang, H. Li, X. Hu, and S. Han, *J. Phys. Chem. A*, 2006, **110**, 7690–5.
49. S. S. Iyengar, H. B. Schlegel, and G. A. Voth, *J. Phys. Chem. A*, 2003, **107**, 7269–7277.
50. M. a. El-Kemary, H. S. El-Gezawy, H. Y. El-Baradie, and R. M. Issa, *Chem. Phys.*, 2001, **265**, 233–242.
51. S. Nosé, *J. Chem. Phys.*, 1984, **81**, 511.
52. W. G. Hoover, *Phys. Rev. A*, 1985, **31**, 1695–1697.
53. R. F. W. Bader, *J. Phys. Chem. A*, 1998, **5639**, 7314–7323.
54. R. F. W. Bader, *Chem. Rev.*, 1991, **91**, 893–928.
55. D. Cremer and E. Kraka, *Angew. Chemie Int. Ed. English*, 1984, **23**, 627–628.
56. C. F. Matta, J. Hernández-Trujillo, T.-H. Tang, and R. F. W. Bader, *Chemistry*, 2003, **9**, 1940–51.
57. N. K. V Monteiro and C. L. Firme, *J. Phys. Chem. A*, 2014, **118**, 1730–1740.
58. C. L. Firme, O. a. C. Antunes, and P. M. Esteves, *Chem. Phys. Lett.*, 2009, **468**, 129–133.
59. K. B. Wiberg, *Acc. Chem. Res.*, 1996, **29**, 229–234.
60. P. E. Eaton and T. W. Cole, *J. Am. Chem. Soc.*, 1964, **86**, 3157–3158.

